Concentration quenched luminescence and energy transfer analysis of Nd^{3+} ions doped Ba-Al-metaphosphate laser glasses

Atul D. Sontakke, Kaushik Biswas, Ashis K. Mandal, K. Annapurna*
Glass Science and Technology Section, Central Glass and Ceramic Research Institute
(*Council of Scientific and Industrial Research*)
196, Raja S.C. Mullick Road, Kolkata - 700032, India

Abstract

This paper reports the dopant ion (Nd^{3+}) concentration effects on its luminescence properties in a new glass system based on barium-alumino-metaphosphates. Amongst the studied concentrations range of 0.276 – 13.31 x 10^{20} ions/cm^3, the glass with 2.879 x 10^{20} ions/cm^3 (1 mol%) Nd^{3+}concentration shows intense NIR emission from $^4F_{3/2}$ excited state, followed by a decrease in emission intensity for further increase in Nd^{3+} ion concentration. The observed luminescence quenching is ascribed to Nd^{3+} self-quenching through donor-donor migration assisted cross-relaxation mechanism. The microscopic energy transfer parameters for donor-acceptor energy transfer, C_{DA} and donor-donor energy migration, C_{DD} have been obtained from the theoretical fittings to experimental decay curves and the spectral overlap model respectively. The C_{DD} parameters (x 10^{-39} cm^6/sec) are found to be about three orders greater than that of C_{DA} (x 10^{-42} cm^6/sec) for Nd^{3+} self-quenching in this host, demonstrating the excitation energy migration among donors is due to hopping mechanism. The energy transfer micoparameters obtained in the present study are comparable to the values reported for commercially available laser glasses LHG-8 and Q-98.

PACS: 32.50.+d, 42.70.Hj, 78.55.Qr, 78.40.-q

Keywords: Nd^{3+} luminescence, concentration quenching, energy transfer analysis, metaphosphate glasses

* Corresponding author: Tel.: +91-33 2473 3469; Fax: +91-33 2473 0957
Email : annapurnak@cgcri.res.in (K. Annapurna)

1. Introduction

Nd^{3+}-doped glasses and crystals have extensively been studied for their applications in the development of solid-state laser materials [1-8]. High absorption coefficients, large absorption line-width as well as high emission cross-section at lasing wavelength are some of the basic requirements for an efficient Nd^{3+}-doped laser material. Among solid-state host materials, crystals are advantageous for their high emission cross-section, narrow emission bandwidth and better thermal conductivity [9]. However, the tedious growth process, size limitations in growth, lower allowable concentrations and uneven distribution of active ions constraint their performance especially for high power applications. On the other side, an easy manufacturing in large scale over a variety of compositional and concentration range with high optical quality makes glasses more attractive over crystals. Due to site-to-site differences of Nd^{3+} ions in glasses, an inhomogeneous broadening appears in the absorption spectrum resulting in a wider absorption band for efficient pumping [10].

Among several glasses, phosphate glasses are most commonly used for high power - high energy laser host materials due to their excellent energy storage and extraction characteristics [11, 12]. Keeping this in view, a number of glasses including sodium-phosphate, barium-phosphate, lithium-sodium-lanthanum-phosphate, zinc-metaphosphate, lead-metaphosphate, potassium-alumino-metaphosphate, potassium-barium-alumino-metaphosphate and potassium-magnesium-alumino-metaphosphate glasses have been studied in the past in evaluating their lasing properties [13-18]. Among them, potassium-barium-alumino-metaphosphate and potassium-magnesium-alumino-

metaphosphate glasses are well known for their commercialization [19]. Since, the phosphate glasses are more prone to OH^- absorption during melting process that increases the non-radiative relaxation rate of excited level and lower the energy storage capacity of Nd^{3+} in lasing medium; special techniques have to be applied in the glass manufacturing. It is found from our initial experiments that the alkali-free metaphosphate glasses are less vulnerable for hydroxyl ion (OH^-) impurity. This observation has encouraged us to take up an investigation on a new alkali-free barium-alumino-metaphosphate glass system, which has not been studied so far. In the present work, as a first step, the effects of concentration on the luminescence properties of Nd^{3+} ions in barium-alumino-metaphosphate glasses have been studied through photoluminescence, excitation and decay analysis. In addition, some important physical and optical properties have also been measured and reported here.

2. Experimental

Nd^{3+}-doped barium-alumino-metaphosphate glasses of chemical compositions in mol% (100-x) (20.95BaO-11.72Al_2O_3-56.12P_2O_5-6.79SiO_2-3.91B_2O_3-0.51Nb_2O_5) + xNd_2O_3 (x = 0.1, 0.3, 0.5, 1.0, 1.5, 3.0, 5.0) were prepared by employing the melt quenching technique. All prepared glasses have been labeled as BAP-Nd01 to BAP-Nd50 based on Nd_2O_3 concentration. The reagent grade metaphosphate chemicals such as $Ba(PO_3)_2$ and $Al(PO_3)_3$, and rare earth oxide Nd_2O_3 with 99.99% purity from Alpha-Aesar were used as starting materials for the glass preparation. The thoroughly mixed chemical batches were sintered at 350°C for 6 h to reduce the surface absorbed moisture and make the pre-reacted batch. Each sintered batch was then melt at 1350°C in high

purity fused quartz crucibles for 1 h with intermittent stirrings to get homogeneity and later casted them onto preheated graphite molds. The cast glass samples were subsequently transferred to a precise temperature controlled annealing furnace kept at 550°C for annealing to relieve thermal stresses followed by a slow cooling to the room temperature. During glass melting process, the relative atmospheric humidity was maintained below 40%. The annealed glasses were then cut and polished in the form of rectangular plates in dimensions of 15 x 20 x 2 mm^3 for their analysis.

The densities of well-annealed glasses were measured by employing Archimedes' buoyancy principle using water as immersion liquid. Refractive indices of glasses were measured at five different wavelengths (473 nm, 532 nm, 632.8 nm, 1064 nm and 1552 nm) on a Prism Coupler (Model: M2010, Metricon) equipped with respective laser sources. The optical absorption spectra were recorded on a UV-Vis spectrophotometer (Model: Lambda20, Perkin-Elmer) in the wavelength range of 200 - 1100 nm. The Photoluminescence, excitation and decay measurements were carried out on a Fluorescence spectrophotometer (Model: Quantum Master-enhanced NIR, from Photon Technologies International) fitted with double monochromators on both excitation and emission channels. The instrument is equipped with LN_2 cooled gated NIR photo-multiplier tube (Model: NIR-PMT-R1.7, Hamamatsu) as detector for acquiring the data from both study state spectra and phosphorescence decay. For performing decay measurements, a 60W Xenon flash lamp was employed as an excitation source. All the measurements were carried out by placing the samples at 60^0 to the incident beam and the signals were collected at right angle to the incident beam from same surface.

3. Results and Discussion

3.1. Physical and Optical Properties

Some of the important physical and optical properties of Nd^{3+}-doped barium-alumino-metaphosphate glasses calculated from their measured density and refractive indices using relevant expressions are presented in Table 1. Density and other related properties show variations in accordance with the increase of Nd^{3+} ion concentration in glasses. The refractive indices at standard wavelengths n_e (at 546.1 nm), $n_{F'}$ (at 480 nm) and $n_{C'}$ (at 643.8 nm) have been estimated from the dispersion curves, Fig. 1, obtained by fitting the measured refractive indices with the five coordinate Sellmeier equation [20],

$$n^2 = A + \frac{B\lambda^2}{\lambda^2 - C} + \frac{D\lambda^2}{\lambda^2 - E} \tag{1}$$

where, n is refractive index at wavelength λ. Abbe number of all the glasses is in the range of 66 – 71, signifying the low optical dispersion and non-linear properties of these glasses.

3. 2. Spectral Properties

3. 2.1. Optical Absorption Spectra

The room temperature UV-visible optical absorption spectra of different Nd^{3+}-doped barium-alumino-metaphosphate glasses are shown in Fig. 2. The spectra have revealed eleven inhomogeneously broadened absorption bands due to *f-f* electronic transitions of Nd^{3+} ions. All the absorption bands have been appropriately assigned depending on their peak energies as illustrated in figure [21]. The absorption peak intensity increases linearly with an increase in Nd^{3+} ion concentration; however, the UV band edge is unaffected with concentration, which is found to be 4.12 eV and 3.73 eV for

direct and indirect band gap transitions respectively. From the absorption spectra, it can be seen that the absorption band due to $^4I_{9/2} \rightarrow {}^4F_{5/2}$, transition at 803 nm in the NIR region has displayed a prominent intensity, which can be used to excite these Nd^3-doped glasses for rich NIR emissions from them.

3. 2. 2 Emission and Excitation Spectra

The room temperature photoluminescence spectra of all the Nd^{3+}-doped barium-alumino-metaphosphate glasses have been recorded on exciting the $^4F_{5/2}$ level at 806 nm. The spectra have demonstrated three emission bands centered at 887 nm, 1058 nm and 1324 nm due to the transitions of $^4F_{3/2} \rightarrow {}^4I_{9/2,\ 11/2\ \&\ 13/2}$ respectively for all glasses. Fig. 3 shows the emission spectrum of BAP-Nd10 glass as a specimen profile and the inset of Fig. 3 depicts the variation of emission intensities with Nd^{3+} concentration. It is clear that, the glass with 1 mol % Nd_2O_3 possesses an intense emission and the fluorescence intensity decreases for the glasses with any further increase in Nd^{3+} concentration. This effect of luminescence quenching due to dopant concentration can also be realized from the excitation spectra presented in Fig. 4, which show the increase in excitation bands intensity up to 1 mol% of Nd_2O_3 and then a decrease for any further increase in the dopant ion concentration in the glasses. This reduction in the fluorescence intensity at higher Nd^{3+} concentrations can be attributed to Nd^{3+} self-quenching (concentration quenching) due to cross-relaxation processes, which may be enhanced with the migration of excitation energy among the active ions [22]. For Nd^{3+} ions, the cross-relaxation processes involve the de-population of emitting $^4F_{3/2}$ level via the transitions $^4F_{3/2}$:$^4I_{9/2} \rightarrow {}^4I_{15/2}$:$^4I_{15/2}$ and $^4F_{3/2}$:$^4I_{9/2} \rightarrow {}^4I_{13/2}$:$^4I_{15/2}$; while the energy migration involves the exodus of

excitation between the excited and nearest neighbor ground state Nd^{3+} ions through $^4F_{3/2}$:$^4I_{9/2} \rightarrow {}^4I_{9/2}$:$^4F_{3/2}$ transitions. A thorough investigation of the observed fluorescence self-quenching in the present Nd^{3+} glass series at higher concentrations has been carried out by means of their fluorescence decay analysis.

3.3 Fluorescence Decay and Energy Transfer Analysis

The normalized fluorescence decay profiles of 1058 nm emission ($^4F_{3/2} \rightarrow {}^4I_{11/2}$) of Nd^{3+} ions in all barium-alumino-metaphosphate glasses are shown in Fig. 5. The measured decay curves are nearly single exponential in nature. The fluorescence decay times (τ) for $^4F_{3/2}$ excited level of all Nd^{3+}- glasses have been obtained from decay curves using the standard expression [22] and are tabulated in Table 2 along with the decay rate ($W = \tau^{-1}$). From the data in Table 2, it can be noticed that the fluorescence decay time decreases with the increase in Nd^{3+} ion concentration. This decrease in fluorescence decay time as a function of Nd^{3+} concentration may be due the energy transfer among dopant ions. Apart from the above mentioned energy transfer processes such as cross-relaxation and energy migration, other energy transfer mechanisms which may influence fluorescence decay time of the excited state is energy re-absorption (radiative trapping). For Nd^{3+} ions, the re-absorption is expected to occur due to the radiative energy transfer between excited Nd^{3+} ions and ground state ions. If this persists, the intensity of emission peak due to $^4F_{3/2} \rightarrow {}^4I_{9/2}$ decreases rapidly with an increase in intensity of transition $^4F_{3/2} \rightarrow {}^4I_{11/2}$ [23]. But it is found that, the relative ratio of integrated emission intensity for these two transitions ($^4F_{3/2} \rightarrow {}^4I_{11/2}$ / $^4F_{3/2} \rightarrow {}^4I_{9/2}$) show no significant variation with the concentration change indicating a negligible amount of re-absorption of emission even if

any that might not have affected the decay kinetics. Hence, the observed decrease in measured fluorescence lifetime with the increase in concentration of Nd^{3+} ions in these glasses has been consider to be due to the excited energy migration assisted energy transfer which has led to the self-quenching at higher concentrations.

The experimental fluorescence decay rate, τ^{-1} of $^4F_{3/2}$ excited level can be expressed as [24],

$$\tau^{-1} = A_{rad} + W_{MP} + W_{ET} \tag{2}$$

where, A_{rad} - radiative decay rate, W_{MP} - nonradiative decay rate due to multi-phonon relaxation and W_{ET} - nonradiative decay rate due to the energy transfer among donor and acceptor (here donor and acceptors are identical ions, i.e. Nd^{3+} ions in $^4F_{3/2}$ excited state are energy donors and those in $^4I_{9/2}$ ground state are acceptors). The inset of Fig. 5 shows a plot of fluorescence decay rate as a function of the square of Nd^{3+} ion concentration in these glasses. It was observed that the fluorescence decay rate exhibits a quadratic dependence on Nd^{3+} ion concentration.

Generally, at very low donor concentration, the donor-donor interactions become almost negligible and in such a condition, the donor luminescence decay exhibits a non-exponential profile, which can be explained through a non-interacting model based on the direct donor to acceptor energy transfer mechanism. Here, the energy transfer rate exhibits a linear dependence on the acceptor ion concentration and will not be affected by donor concentration [25, 26]. However, at higher donor concentrations, the donor-donor energy transfer becomes dominant over donor-acceptor energy transfer. This will cause a

superfast excitation migration among the donors before the actual donor-acceptor energy transfer, which will occur only at shortest possible distance between donor and acceptor. This is called as a super-migration region [25, 27] where, the decay profile exhibits exponential nature and the energy transfer rate linearly depends on the acceptor ion concentration alone. Apart from these two extreme situations, an intermediate case does exist. In this case, the energy transfer is assisted with donor-donor migration but the energy transfer rate shows a linear dependence with the product of acceptor and donor ion concentrations [27]. Since, the experimental fluorescence decay rate is proportional to the square of Nd^{3+} ion concentration in the present Nd^{3+} glass system (inset of Fig. 5); it ascertains the energy transfer is assisted with donor energy migration [24].

In order to examine the actual energy transfer mechanism involved, the microscopic energy transfer parameters for donor-donor energy migration (C_{DD}) and donor-acceptor energy transfer (C_{DA}) have been derived by adopting two approaches based on the spectral overlap model and the donor fluorescence decay kinetics respectively. According to the Forster-Dexter theory, the energy transfer between donor and acceptor depends on the spectral overlap of donor's emission and acceptor's absorption [28]. By applying this spectral overlap model to $^4F_{3/2} \leftrightarrow {}^4I_{9/2}$ transitions, we have obtained the microscopic energy transfer parameter for Nd^{3+} donor-donor energy migration, C_{DD} using the relation [29] as given below,

$$C_{DD} = \frac{3c}{8\pi^4 n^2} \int \sigma_{abs}^{D}(\lambda)\sigma_{em}^{D}(\lambda)d\lambda \qquad (3)$$

where, c is velocity of light in vacuum and $\sigma_{abs}^{D}(\lambda)$, $\sigma_{em}^{D}(\lambda)$ are absorption and emission cross-sections of $^4F_{3/2} \leftrightarrow {}^4I_{9/2}$ transitions of Nd^{3+} ion respectively. The absorption cross-section can be obtained from the absorption spectrum by using the relation [30],

$$\sigma_{abs}^{D}(\lambda) = \frac{2.303a(\lambda)}{N_{Nd}\, l} \tag{4}$$

where, $a(\lambda)$ is the absorbance at wavelength λ, N_{Nd} is Nd^{3+} ion concentration and l is the sample path length. The experimental absorption cross-section spectrum for $^4I_{9/2} \rightarrow {}^4F_{3/2}$ transition is as shown in Fig. 6. This figure also projects the emission cross-sections for $^4F_{3/2} \rightarrow {}^4I_{9/2}$ transition, which were obtained by using two methods such as McCumber's reciprocity method, and the Fuchtbauer-Ladenburg (F-L) method, following the empirical formulae as given below respectively [31-32],

$$\sigma_{em}^{D}(\lambda) = \frac{Z_l}{Z_u}\sigma_{abs}^{D}(\lambda)\exp\left[\frac{E_{ZL} - E_{\lambda}}{K_B T}\right] \tag{5}$$

$$\sigma_{em}^{D}(\lambda) = \frac{\lambda^5 \beta}{8\pi n^2 c\, \tau_{rad}} \frac{I(\lambda)}{\int \lambda I(\lambda) d\lambda} \tag{6}$$

where, Z_l and Z_u are the degeneracy of lower and upper transition levels respectively, E_{ZL} is the energy separation between lowest components of lower and upper states, E_λ is the energy at wavelength λ, K_B is Boltzmann constant, T is absolute temperature, τ_{rad} is the radiative decay time and β is branching ratio for $^4F_{3/2} \rightarrow {}^4I_{9/2}$ transition. The emission cross-section spectra obtained using both the methods have been used for the calculation of energy transfer micro-parameters. The energy transfer micro-parameter, C_{DD} values obtained by using the reciprocity method is 3.8 x 10^{-39} cm^6/sec and from the F-L model is 3.2 x 10^{-39} cm^6/sec which is in close agreement.

The energy transfer micro-parameter, C_{DA}, for donor-acceptor energy transfer by cross-relaxation mechanism, has been obtained based on the donor luminescence decay analysis using different theoretical models. According to previous reports, energy transfer between Nd^{3+} ions is mainly due to dipole-dipole electrostatic interactions [19, 33-35]. Thus, by considering the dipole-dipole interactions among Nd^{3+} ions, the donor fluorescence decay spectrum have been analyzed using direct donor-acceptor energy transfer based Inokuti-Hirayama relation [26] as given below,

$$I(t) = I_0 \exp\left[-\frac{t}{\tau_0} - \frac{4\pi}{3} N_A \Gamma\left(1 - \frac{3}{s}\right)\left(C_{DA} t\right)^{3/s} \right] \quad (7)$$

where, τ_0 is the intrinsic fluorescence decay time of donor luminescence , $\Gamma(1-3/s)$ is Euler's gamma function, N_A is acceptor ion concentration, C_{DA} is donor-acceptor energy transfer micro-parameter and s is multipole interaction parameter (s = 6 for dipole-dipole interactions). Fig. 7 shows the theoretical fittings generated using Eq. 7 to the experimental decay curves for different Nd^{3+}-doped glasses under study. From this figure it is clear that, the theoretical curves are fitting well with the experimental data for the glasses with Nd_2O_3 concentration up to 0.5 mol%. However, for BAP-Nd10 glass, the fit shows partial deviation from the experiment, which increases for further increase in dopant ion concentration. This deviation of Inokuti-Hirayama model from experimental curve demonstrates the energy transfer is not direct donor-acceptor but involves some energy migration among the dopant ions, which becomes more significant at higher Nd^{3+} concentrations. In order to establish this, two other models such as Yokota-Tanimoto, Eq. (8) and Burshtein, Eq. (9) have been used for the analysis of decay curves at higher Nd^{3+} concentrations. These two models give a general solution for donor luminescence decay

function by assuming the energy transfer from donor to acceptor is assisted with donor-donor energy migration either by diffusion or by hopping process, and are as given below [27, 36, 37],

$$I(t) = I_0 \exp\left[-\frac{t}{\tau_0} - \frac{4\pi}{3} N_A \Gamma\left(1-\frac{3}{s}\right)\left(C_{DA} t\right)^{3/s} \left(\frac{1+10.87X+15.5X^2}{1+8.74X} \right)^{\frac{s-3}{s-2}} \right] \tag{8}$$

$$\text{where, } X = DC_{DA}^{-2/s} t^{1-2/s} \text{ And } D = \frac{1}{2}\left(\frac{4\pi N_D}{3}\right)^{4/3} C_{DD}$$

$$I(t) = I_0 \exp\left(-\frac{t}{\tau_0} - \frac{4\pi}{3} N_A \Gamma\left(1-\frac{3}{s}\right)\left(C_{DA} t\right)^{3/s} - W_m t \right) \tag{9}$$

where, W_m is migration rate, D is diffusion coefficient, N_D is donor ion concentration and C_{DD} is donor-donor energy migration micro-parameter. The theoretical fits generated using both Yokota-Tanimoto and Burshtein models are also presented in the Fig. 7, exhibiting good agreement with the experimental decay curves. From the figure it is clear that, for lower concentrations ($\leq$ 0.5 mol% Nd_2O_3), the migration/diffusion parameters are insignificant and hence the above relations for both the models resemble to that of Inokuti-Hirayama model (Eq. 7), suggesting the direct donor - acceptor energy transfer path at Nd^{3+} concentration less than or equal to 1.37 x 10^{20} ions/cm^3 (0.5 mol%), above which the energy transfer is through donor-donor migration assisted cross-relaxation mechanism. The energy transfer micro-parameter (C_{DA}), diffusion coefficient (D) and migration rate (W_m) obtained from these theoretical fittings are listed in Table 3 along with the critical distance (R_0) for luminescence quenching [38] obtained from relation,

$$R_0 = \left(C_{DA}\tau_0\right)^{1/6} \tag{10}$$

From Table 3, the average value of donor-acceptor energy transfer micro-parameter is found to be in the range of 3-8 x 10^{-42} cm^6/sec. Thus, the energy transfer micro-parameter for donor-donor energy migration, C_{DD} (x 10^{-39} cm^6/sec) is almost three orders of magnitude greater than that of donor-acceptor energy transfer micro-parameter, C_{DA} (x 10^{-42} cm^6/sec) signifying the migration assisted cross relaxation based energy transfer at higher concentrations for Nd^{3+} self-quenching in barium-alumino-metaphosphate glasses, which are in accordance to the values reported for commercial phosphate laser glasses, Q-98 and LHG-8 [22]. Since, $C_{DD} >> C_{DA}$, the energy transfer follows the hopping migration and not the diffusion, suggesting Burshtein's model is more appropriate.

Generally, the hopping model is applicable when the energy migration among donors is stronger than the direct donor–acceptor energy transfer and the diffusion model is applicable when the energy migration between donors is significant but does not dominate the energy transfer. Interestingly, both Burshtein's hopping model and Yokota-Tanimoto's diffusion model could simulate good fits to the experimental data (with regression coefficient close to 1) as shown in Fig. 7. Such observation has been reported in the literatures [39 - 41] where both the models exhibited good fittings to the decay curves for migration assisted energy transfers and thus, it often creates an uncertainty in the selection of real migration mechanism. Yokota-Tanimoto model has been further investigated to calculate the C_{DD} micro-parameter using the diffusion coefficient, D. The values obtained are in the range of 0.4 – 0.7 x 10^{-39} cm^6/sec, which are sharply deviating from the C_{DD} calculated using the spectral overlap model (~3.5 x 10^{-39} cm^6/sec). Hence, this marked difference in the C_{DD} parameters obtained from spectral overlap model and

Yokota-Tanimoto model may be due to the inappropriateness of diffusion based Yokota-Tanimoto model in the present system. For further confirmation of the migration mechanism i. e. diffusion or hopping, the theoretical energy transfer rates k_d and k_h have been calculated (Table 4) based on the diffusion and hopping migration respectively and compared with the experimental energy transfer rate k_{exp} [28, 30]. Here $k_{exp} = \{[(C_{DA} + C_{AD})/ C_{DA}] \times (\tau^{-1} - A_{rad})\}$, where, C_{AD} stands for energy back transfer from acceptor to donor [30]. For Nd^{3+} ions the probability of energy back transfer from $^4I_{15/3}$ level to $^4F_{3/2}$ level can be ruled out owing to the fast multi-phonon relaxation of $^4I_{15/2}$ level to the lower levels. According to Jagosich et al. [39], the donor energy migration defining parameter, R ($=k_{exp}/k_d$) should be equal to one for diffusion mechanism and less than one for hopping mechanism. Table 4 presents the calculated values of R, which are less than one for the samples with high Nd^{3+} concentrations ascertaining the hopping mechanism based migration assisted energy transfer among Nd^{3+} ions to occur leading to fluorescence quenching in them.

4. Conclusions

In summary, we conclude that a new series of highly transparent barium-alumino-metaphosphate glasses containing Nd_2O_3 in varied contents from 0.1 to 5 mol% ($0.276 - 13.31 \times 10^{20}$ ions/cm^3), have successfully been prepared and studied for the effect of concentration on their luminescence properties. Upon excitation with 806 nm, an intense emission at 1058 nm due to the transition of $^4F_{3/2} \rightarrow {}^4I_{11/2}$ of Nd^{3+} has been realized from all the glasses. Especially a glass with 1 mol% Nd_2O_3 has displayed maximum fluorescence intensity and beyond that concentration, luminescence quenching

has been observed. The luminescence decay analysis has been carried out by using different theoretical models such as Inokuti-Hirayama, Yokota-Tanimoto and Burshtein models in order to understanding the energy transfer mechanisms involved. The classical Inokuti-Hirayama model for direct donor-acceptor energy transfer mechanism accounts well for the experimental decay curves at low concentration but deviates at higher Nd^{3+} concentration. This deviation at higher concentrations has been successfully illustrated as due to the contribution of donor excitation energy migration in energy transfer mechanism through the theoretical fittings using Burshtein' hopping and Yokota-Tanimoto's diffusion models. The energy transfer micro-parameter for donor-donor energy migration (~3.5 x 10^{-39} cm^6/sec) is found to be almost three orders of magnitudes greater than donor-acceptor energy transfer micro-parameter (~3-8 x 10^{-42} cm^6/sec) for Nd^{3+} ions in the studied glasses, which confirmed the hopping migration assisted energy transfer at higher Nd^{3+} concentrations. Hence, it is suggested that, the energy transfer among Nd^{3+} ions follows the direct donor-acceptor cross-relaxation ($^4F_{3/2}$:$^4I_{9/2}$ → $^4I_{15/2}$:$^4I_{15/2}$) path at low concentration (≤ 1.37 x 10^{20} ions/cm^3), however at higher concentrations it is assisted with the donor-donor migration ($^4F_{3/2}$:$^4I_{9/2}$ → $^4I_{9/2}$:$^4F_{3/2}$) in the present Ba-Al-metaphosphate glasses.

Acknowledgements

Authors would like to thank Director, CGCRI for his kind encouragement and permission to publish this work that was carried out in an In-house project No. MLP0101. Our thanks are also due to Dr. Ranjan Sen, Head, Glass Division for his support in the present work. One of us (Mr.A.D.S.) is thankful to the CGCRI, CSIR for the award of Research Internship to him.

References

[1] S. A. Payne, C. D. Marshall, A. Bayramian, G. D. Wilke, J. S. Hayden, Appl. Phys. B 61, 257 (1995)

[2] J. R. Thornton, W. D. Fountain, G. W. Flint, T. G. Crow, Appl. Optics 8, 1087 (1969)

[3] T. T. Basiev, Sov. J. Quantum electron. 13, 370 (1983)

[4] A. G. Avanesov, Yu. K. Voron'ko, B. I. Denker, G. V. Maksimova, V. V. Osiko, A. M. Prokhorov, I. A. Schherbakov, Sov. J. Quantum Electron. 9, 935 (1979)

[5] B. I. Denker, V. V. siko, P. P. Pashinin, A. M. Prokhorov, Sov. J. Quantum Elctron. 11, 289 (1981)

[6] C. Tu, Z. Zhu, J. Li, Y. Huang, B. Wu, M. Huang, Z. Chen, Opt. Mater. 27, 167 (2004)

[7] J. H. Campbell, T. I. Suratwala, J. Non-Crystal. Solids 263-64, 318 (2000)

[8] A. A. Kaminskii, K. Ueda, N. Uehara, Jap. J. Appl. Phys. 32, L586 (1993)

[9] T. W. Pollak, W. F. Wing, R. J. Grasso, E. P. Chicklis, H. P. Jenssen, IEEE J. Quantum Electron. 18, 159 (1982)

[10] A. G. Avanesov, Yu. G. Basov, V. G. Garmash, B. I. Denker, N. N. Il'ichev, G. V. Maksimova, A. A. Malyutin, V. V. Osiko, P. P. Pashinin, A. M. Prokhorov, V. V. Sychev, Sov. J. Quantum Electron. 10, 644 (1980)

[11] J. L. Emmett, W. F. Krupke, J. B. Trenholme, Report UCRL -53344 (Lawrence-Livermore National Laboratory, Livermore, CA, 1982)

[12] B. M. VanWonterghem, J. R. Murray, J. H. Campbell, D. R. Spek, C. M. Barker, L. C. Smith, D. F. browning, W. C. Behrendt, Appl. Opt. 36, 4932 (1997)

[13] J. Dong, M.Bass, G. Walters, J. Opt. Soc. Am. B 21, 454 (2004)

[14] Y. M. Moustafa, K El-Egili, J. Non-Cryst. Solids 240, 144 (1998)

[15] A. G. Avanesov, I. V. Vasil'ev, Yu. K. Voron'ko, B. I. Denker, S. V. Zinov'ev, A. S. Kuznetsov, V. V. Osiko, P. P. Pashinin, A. M. Prokhorov, A. A. Semenov, Sov. J. Quantum Electron. 9, 937 (1979)

[16] I.E.C. Machado, L. Prado, L. Gomes, J.M. Prison and J.R. Martinelli, J. Non-Cryst. Solids 348, 113 (2004)

[17] J. A. Capobianco, P. P. Proulx, M. Bettinelli, F. Negrisolo, Phys. Rev. B 42, 4936 (1990)

[18] A. R. Kuznetsov, S. G. Lunter, S. I. Nikitina, A. G. Plyukhin and Yu. K. Fedorov, J. Appl. Spectroscopy 56, 90 (1992)

[19] P. R. Ehrmann, J. H. Campbell, J. Am. Ceram. Soc. 85, 1061 (2002)

[20] W. El Shirbeeny, M. H. Aly, A. E. El-Samahy, K. M. Emad, Int. J. Pure & Appl. Phys. 3, 122 (2007)

[21] W. T. Carnall, P. R. Fields, K. Rajnak, J. Chem. Phys. 49, 4424 (1968)

[22] C. Jacinto, S. L. Oliveira, L. A. O. Nunes, J. D. Myers, M. J. Myers, T. Catunda, Phys. Rev. B 73, 125107-1 (2006)

[23] J. A. Caird, A. J. Ramponi, P. R. Staver, J. Opt. Soc. Am. B 8, 1391 (1991)

[24] M. C. Nostrand, R. H. Page, S. A. Payne, L. I. Isaenko, A. P. Yelisseyev, J. Opt. Soc. Am. B 18, 264 (2001)

[25] D. L. Huber, Phys. Rev. B, 20 2307 (1979)

[26] M. Inokuti, F. Hirayama, J. Chem. Phys. 43, 1978 (1965)
[27] A. I. Burshtein, Sov. Phys. JETP 35, 882 (1972)
[28] D. L. Dexter, J. Chem. Phys. 21, 836 (1953)
[29] A. Braud, S. Girald, J. L. Doualan, R. Moncorge, IEEE J. Quantum Electron. 34, 2246 (1998)
[30] C Hu, FE Muller-Karger, RG Zepp, Limnol. Oceanogr. 47, 1261 (2002)
[31] L. R. P. Kassab, M. E. Fukumoto, L. Gomes, J. Opt. Soc. Am. B 22, 1255 (2005)
[32] F. Liegard, J. L. Doualan, R. Moncorge, M. Bettinelli, Appl. Phys. B 80, 985 (2005)
[33] L. D. Merkle, M. Dubinskii, K. L. Schepler, M. Hegde, Opt. Express 14, 3893 (2006)
[34] T. T. Basiev, Y. V. Orlovskii, Y. S. Privis, J. Lumin. 69, 187 (1996)
[35] V. Lupei, Opt. Mater. 16, 137 (2001)
[36] M. Yokota, O. Tanimoto, J. Phys. Soc. Japan 22, 779 (1967)
[37] I. R. Martin, V. D. Rodriguez, U. R. Rodriguez-Mendoza, V. Lavin, E. Montoya, D. Jaque, J. Chem. Phys. 111, 1191 (1999)
[38] L. D. da Vila, L. Gomes, L. V. G. Tarelho, S. J. L. Ribeiro, Y. Messedeq, J. Appl. Phys. 93, 3873 (2003)
[39] F. H. Jagosich, L. Gomes, L. V. G. Tarelho, L. C. Courrol, I. M. Ranieri, J. Appl. Phys. 91, 624 (2002)
[40] Y. Liu, Y. Chen, Y. Lin, Q. Tan, Z. Luo, Y. Huang, J. Opt. Soc. Am. B 24, 1046 (2007)
[41] C. M. Lawson, E. E. Freed, R. C. Powell, J. Chem. Phys. 76, 4171 (1982)

Table Captions

Table 1: Important physical and optical properties; density (d), average molecular weight (M_{avg}), molar volume (V_M), Nd^{3+} ions concentration (N_{Nd}), inter-ionic distance (r_i), polaron radius (r_p), field strength (F), refractive index (n_e, $n_{F'}$ and $n_{C'}$), Abbe number (v_e) and reflection loss ($R\%$) of all Nd^{3+}-doped Ba-Al-metaphosphate glasses.

Table 2: Fluorescence decay time (τ), average decay rate (W) and energy transfer rate (W_{ET}) of 1058 nm emission of different Nd^{3+}-doped Ba-Al-metaphosphate glasses.

Table 3: The experimental values of Energy transfer micro-parameter (C_{DA}, C_{DD}), Critical distance (R_0), Diffusion coefficient (D) and energy migration rate (W_m) obtained from theoretical fits and spectral overlap models for different Nd^{3+}-doped Ba-Al-metaphosphate glasses. (R^2 stands for regression coefficient from theoretical fits)

Table 4: Theoretical energy transfer rates for diffusion (k_d) and hopping (k_h) migrations and the energy transfer defining parameter R (= k_{exp}/k_d) for Nd^{3+}-doped Ba-Al-metaphosphate glasses.

Figure Captions

Fig. 1: Dispersion curves obtained using the Sellmeier relation for all Nd^{3+}-doped Ba-Al-metaphosphate glasses.

Fig. 2: Optical absorption spectra of Nd^{3+}-doped Ba-Al-metaphosphate glasses.

Fig. 3: Fluorescence spectrum of Nd^{3+}-doped Ba-Al-metaphosphate glass, BAP-Nd10 on 806 nm excitation. (Inset: Plot of variation of emission intensities with Nd_2O_3 concentration)

Fig. 4: Excitation spectra of Nd^{3+}-doped Ba-Al-metaphosphate glasses on monitoring the 1058 nm emission.

Fig. 5: Normalized fluorescence decay spectra of 1058 nm emission of Nd^{3+}-doped Ba-Al-metaphosphate glasses on excitation at 806 nm. (Inset: Plot of fluorescence decay rate with square of Nd^{3+} ion concentration)

Fig. 6: Spectral overlap of absorption and emission cross-sections for $^4F_{3/2} \leftrightarrow {}^4I_{9/2}$ transitions of Nd^{3+} ions in Ba-Al-metaphosphate glasses.

Fig. 7: Semi-log plot of decay curves for Nd^{3+}-doped Ba-Al-metaphosphate glasses.

Table 1

Glass	BAP-Nd01	BAP-Nd03	BAP-Nd05	BAP-Nd10	BAP-Nd15	BAP-Nd30	BAP-Nd50
Physical Properties							
d (g/cm^3)	3.021	3.022	3.025	3.036	3.062	3.093	3.141
M_{avg} (g/mol)	132.1	132.5	132.9	134.0	134.9	138.0	142.1
V_M (cm^3)	43.7	43.8	43.9	44.1	44.1	44.6	45.2
N_{Nd} (x10^{20} cm^{-3})	0.276	0.824	1.371	2.879	4.100	8.097	13.31
r_i (Å)	33.10	22.98	19.39	15.15	13.46	10.73	9.09
r_p (Å)	13.34	9.26	7.82	6.11	5.42	4.32	3.66
F (10^{14} cm^{-2})	1.68	3.50	4.91	8.05	10.19	16.047	22.35
Optical Properties							
n_e	1.5514	1.5516	1.5518	1.5529	1.5555	1.5579	1.5621
$n_{F'}$	1.5552	1.5556	1.5558	1.5566	1.5596	1.5621	1.5663
$n_{C'}$	1.5474	1.5475	1.5478	1.5490	1.5514	1.5537	1.5579
v_e	70.7	70.5	70.3	70.0	69.3	68.2	66.6
R%	4.67	4.67	4.68	4.69	4.73	4.76	4.81

Table 2

Glass	τ (μsec)	W (sec^{-1})	W_{ET} (sec^{-1})
BAP-Nd01	318.4	3140	216.5
BAP-Nd03	312.9	3196	271.9
BAP-Nd05	306.2	3266	341.8
BAP-Nd10	283.6	3526	602.1
BAP-Nd15	242.9	4217	1192.2
BAP-Nd30	166.8	5992	3071.2
BAP-Nd50	93.2	10730	7805.6

Table 3

Glass	C_{DA} (10^{-42} cm^6sec^{-1})	R_0 (Å)	D (10^{-11} cm^2sec^{-1})	W_m (sec^{-1})	Regression Coefficient (R^2)
Inokuti-Hirayama Model					
BAP-Nd01	4.70	3.42	-	-	0.9999
BAP-Nd03	5.70	3.53	-	-	0.9999
BAP-Nd05	5.69	3.53	-	-	0.9992
BAP-Nd10	6.02	3.57	-	-	0.9973
Yokota-Tanimoto Model					
BAP-Nd01	-	-	-	-	
BAP-Nd03	-	-	-	-	
BAP-Nd05	8.57	3.78	0.12	-	0.9999
BAP-Nd10	5.40	3.50	0.24	-	0.9999
BAP-Nd15	4.74	3.43	0.80	-	0.9999
BAP-Nd30	4.75	3.43	1.15	-	0.9999
BAP-Nd50	4.86	3.44	2.09		0.9999
Burshtein Model					
BAP-Nd01	-	-	-	-	
BAP-Nd03	-	-	-	-	
BAP-Nd05	7.09	3.66	-	0	0.9999
BAP-Nd10	5.69	3.53	-	200	0.9999
BAP-Nd15	5.14	3.47	-	830	0.9999
BAP-Nd30	4.32	3.37	-	2300	0.9999
BAP-Nd50	3.43	3.25	-	6310	0.9998
Spectral Overlap Model					

Model	C_{DD} (10^{-39} cm^6sec^{-1})	R_0 (Å)
McCumber	3.81	10.4
Fuchtbauer-Ladenburg	3.17	10.2

Table 4

Glass	k_d (sec^{-1})	k_h (sec^{-1})	R (k_{exp}/k_d)
BAP-Nd01	10.4	1.8	20.84
BAP-Nd03	92.9	16.5	2.93
BAP-Nd05	257.0	45.6	1.33
BAP-Nd10	1134.7	201.1	0.53
BAP-Nd15	2299.4	407.6	0.52
BAP-Nd30	8968.7	1589.8	0.34
BAP-Nd50	24237.0	4296.2	0.32

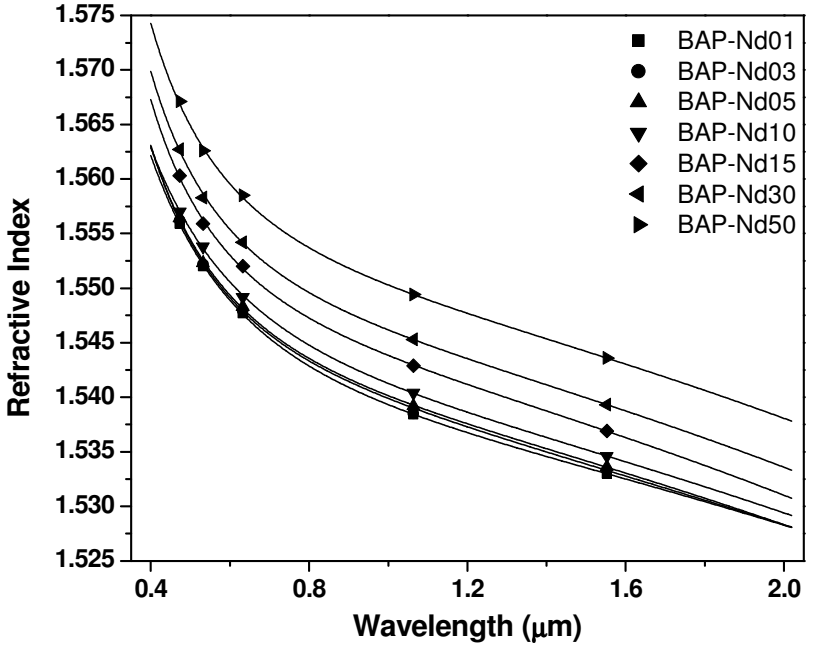
Refractive Index
Wavelength (μm)
BAP-Nd01
BAP-Nd03
BAP-Nd05
BAP-Nd10
BAP-Nd15
BAP-Nd30
BAP-Nd50

Fig. 1

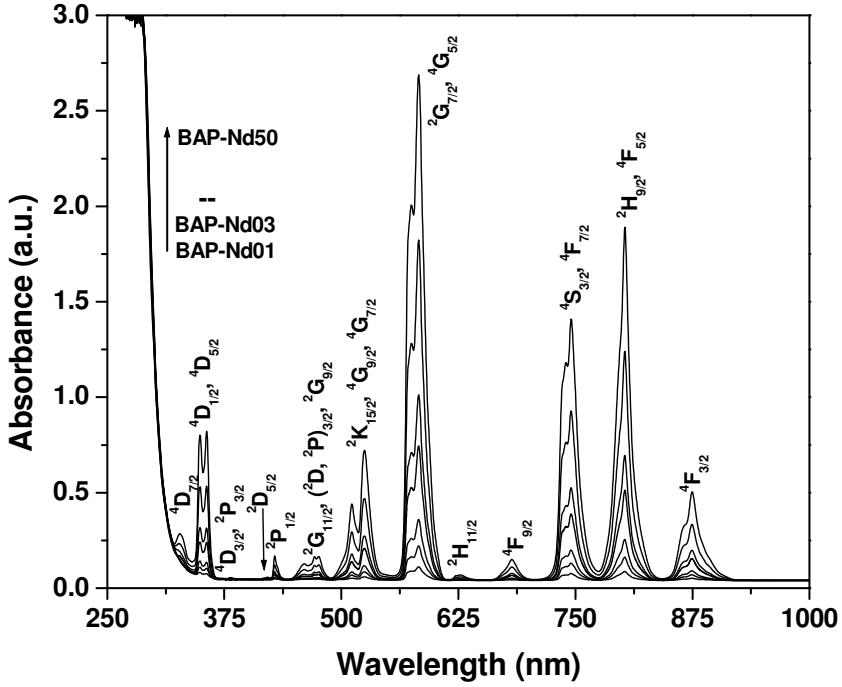
Absorbance (a.u.)
Wavelength (nm)
BAP-Nd50
BAP-Nd03
BAP-Nd01
4D7/2
4D1/2, 4D5/2
2P3/2
2D5/2
4D3/2, 2P1/2
2G11/2, (2D, 2P)3/2, 2G9/2
2K15/2, 4G9/2, 4G7/2
2G7/2, 4G5/2
2H11/2
4F9/2
4S3/2, 4F7/2
2H9/2, 4F5/2
4F3/2

Fig. 2

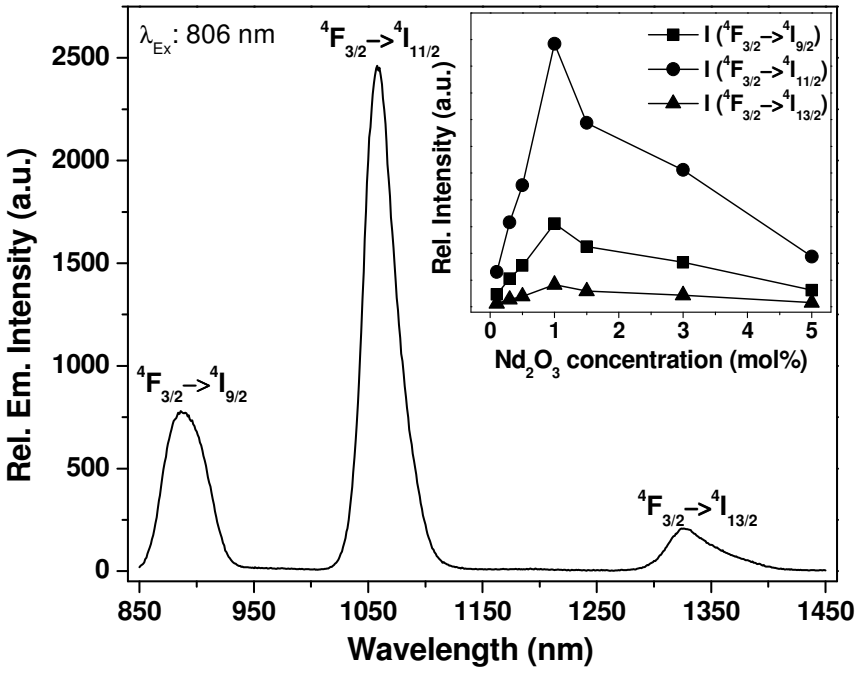
λEx: 806 nm
4F3/2->4I11/2
4F3/2->4I9/2
4F3/2->4I13/2
Rel. Em. Intensity (a.u.)
Wavelength (nm)
I (4F3/2->4I9/2)
I (4F3/2->4I11/2)
I (4F3/2->4I13/2)
Rel. Intensity (a.u.)
Nd2O3 concentration (mol%)

Fig. 3

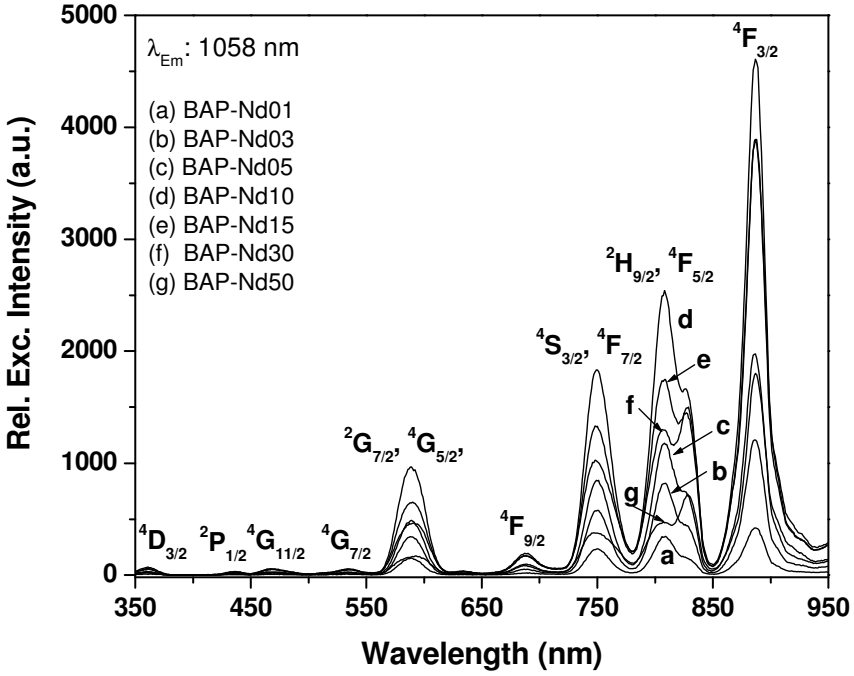
λEm: 1058 nm
(a) BAP-Nd01
(b) BAP-Nd03
(c) BAP-Nd05
(d) BAP-Nd10
(e) BAP-Nd15
(f) BAP-Nd30
(g) BAP-Nd50
4D3/2
2P1/2
4G11/2
4G7/2
2G7/2, 4G5/2,
4F9/2
4S3/2, 4F7/2
2H9/2, 4F5/2
4F3/2
Rel. Exc. Intensity (a.u.)
Wavelength (nm)

Fig. 4

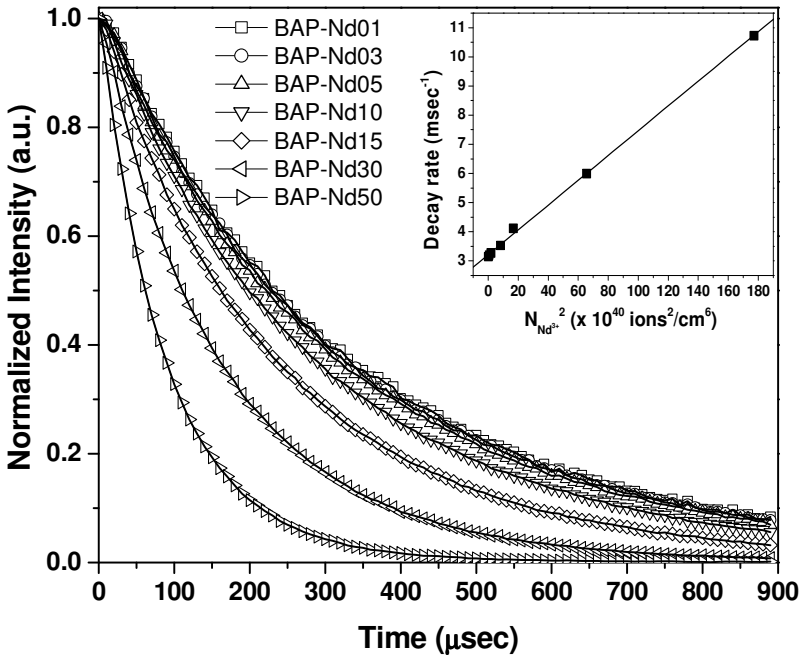
BAP-Nd01
BAP-Nd03
BAP-Nd05
BAP-Nd10
BAP-Nd15
BAP-Nd30
BAP-Nd50
Normalized Intensity (a.u.)
Time (μsec)
Decay rate (msec^{-1})
$N_{Nd^{3+}}{}^2$ (x 10^{40} ions^2/cm^6)

Fig. 5

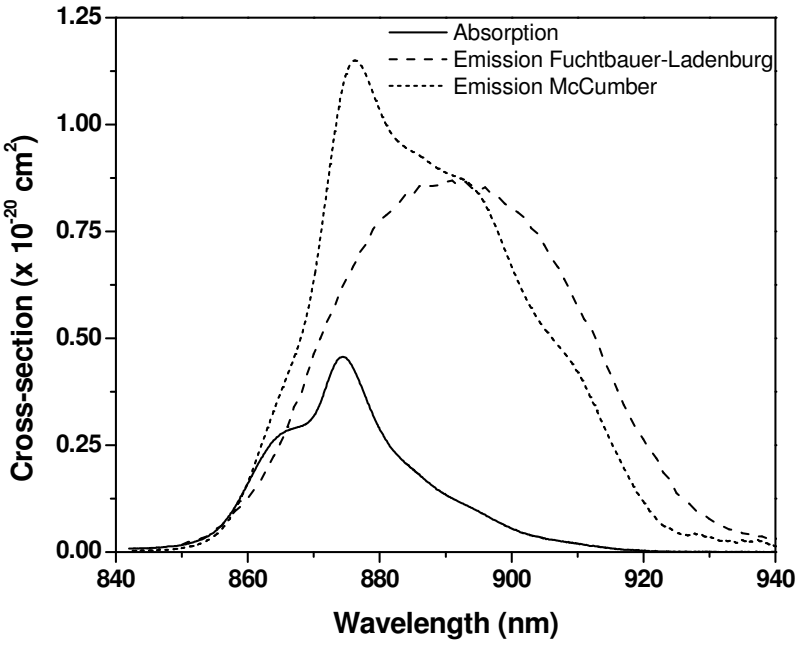
Absorption
Emission Fuchtbauer-Ladenburg
Emission McCumber
Cross-section (x 10^{-20} cm^2)
Wavelength (nm)

Fig. 6

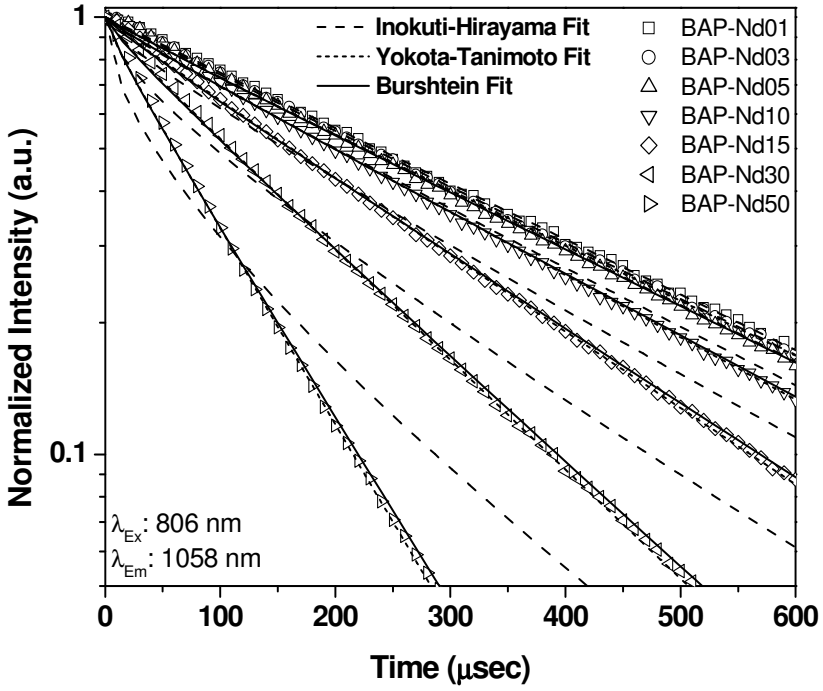
Inokuti-Hirayama Fit
Yokota-Tanimoto Fit
Burshtein Fit
BAP-Nd01
BAP-Nd03
BAP-Nd05
BAP-Nd10
BAP-Nd15
BAP-Nd30
BAP-Nd50
Normalized Intensity (a.u.)
1
0.1
λEx: 806 nm
λEm: 1058 nm
0
100
200
300
400
500
600
Time (μsec)

Fig. 7